

Light-amplified Landau-Zener conductivity in gapped graphene monolayers: a simulacrum of photo-catalyzed vacuum instability

Selym Villalba-Chávez,^{1,*} Oliver Mathiak,^{1,†} Reinhold Egger,^{1,‡} and Carsten Müller^{1,§}

¹*Institut für Theoretische Physik, Heinrich-Heine-Universität Düsseldorf,
Universitätsstr. 1, 40225 Düsseldorf, Germany*

(Dated: November 9, 2022)

Interband transitions of electrons in a gapped graphene monolayer are highly stimulated near the Fermi surface when a high-frequency electric wave of weak intensity and a strong constant electric field are superposed on its surface. We consider the situation in which the photon energy associated with the fast-oscillating field is slightly below the graphene gap so that the quantum transitions still occur through tunneling effects while being facilitated by multiphoton absorption channels. In the considered parameter regime the photo-catalyzed current linked to the described setup is shown to exceed the one driven by the strong field solely by several orders of magnitude. Optimization conditions are revealed and an asymptotic formula for the current density is derived. The robustness of our assessment supports the viability of detecting this phenomenon in graphene, which would serve as a first-principle-proof of concept of the dynamically-assisted Schwinger mechanism in QED.

I. INTRODUCTION

A strong, homogenous electric-like background renders the ground state of quantum electrodynamics (QED) unstable, allowing quantum vacuum fluctuations of the electron-positron field to spontaneously materialize into their mass shells [1–4]. The pair production rate $\mathcal{R} \sim \exp[-\pi m_e^2 c^3 / (e\hbar E)]$ related to this emblematic phenomenon—widely known as the Schwinger mechanism—has a tunneling nature and exhibits, in addition to a nonlinear dependence on the external field E , an essential singularity in the electric charge $e > 0$ which transfers to the process a nonperturbative feature [5–7]. So far, the observation of this field-induced vacuum instability has been prevented by the unavailability of field strengths comparable to the characteristic QED scale $E_{\text{cr}} = m_e^2 c^3 / (e\hbar) \sim 10^{16}$ V/cm, at which the exponential suppression of \mathcal{R} turns out to be mitigated.¹ Although fields of the order of $E \sim 10^{-2} E_{\text{cr}}$ are aimed for by the next generation of multipetawatt laser facilities such as the Extreme Light Infrastructure (ELI) [8] and the Exawatt Center for Extreme Light Studies (XCELS) [9], it is generally believed that an experimental realization of this yet hypothetical vacuum breakdown might represent a major challenging task by the time when both ELI and XCELS become operational. The challenge is that at the envisaged field strengths the production rate remains very small, a fact that calls for alternative routes which relieve the described issue.

While in the last two decades theoretical endeavors to-

ward this goal have provided significant insight about the nontrivial nature of the quantum vacuum [10–17], most notably the scenario first investigated in Refs. [18, 19] has raised the hope of observing the vacuum instability for the first time. In contrast to the traditional single-field scheme, the promising setup relies on a temporal overlapping of a strong homogenous electric field and a weak but high-frequency $\omega \lesssim 2m_e$ electric pulse. This so-called dynamically-assisted Schwinger mechanism retains the tunneling feature while the absorption of quanta induces a reduction of the effective barrier width that an electron has to traverse from the negative to the positive Dirac continuum. This reduction, in turn, should facilitate the production of pairs at a rate $\mathcal{R} \sim \exp[-\kappa\pi E_{\text{cr}}/E]$ that enhances substantially as compared to the case of the standard Schwinger effect because the positive parameter κ could be much smaller than unity. Improvements of various field configurations sharing the described idea have been proposed, including the combination of a static electric field and pulses with or without subcycle structures [20–28], the situation in which two Sauter waves are superposed [29, 30], as well as scenarios in which both the strong and the fast-oscillating fields hold subcycles while being modulated by pulse profiles [31–38]. Furthermore, analogous upgrades have been reported theoretically in both the Bethe-Heitler [39, 40] and Breit-Wheeler [41] pair production process.²

Despite the described advantage, gathering adequate experimental conditions for implementing the dynamically-assisted Schwinger mechanism is not an easy task because strong fields $E \sim E_{\text{cr}}$ are required anyway

*Electronic address: villalba@uni-duesseldorf.de

†Electronic address: Oliver.Mathiak@hhu.de

‡Electronic address: egger@hhu.de

§Electronic address: c.mueller@tp1.uni-duesseldorf.de

¹ Here m_e refers to the electron mass and c to the speed of light. From now on the Planck constant and the vacuum permittivity are set to unity $\hbar = \epsilon_0 = 1$.

² In contrast to the vacuum decay, there exists an experimental confirmation of the nonlinear Breit-Wheeler pair production channel in the few photon regime, where the rate follows a power law scaling with the applied field strength [42]. New campaigns aim to verify the fully nonperturbative regime of this process [see Refs. [43–48]].

for having a sizable production of pairs. Notwithstanding, emergent condensed-matter systems with optoelectronic features that resemble those linked to the QED vacuum might constitute solid state playgrounds for simulating the vacuum instability via transitions of electrons from valence to conduction bands of Landau-Zener nature [49, 50]. However, an essential requirement for assessing a plausible enhancement caused by the absorption of photons of a weak but fast-oscillating electric mode, i.e., the solid state analog of the dynamically-assisted Schwinger mechanism, is the existence of *massive* charge carriers. A graphene monolayer [51–53] with a tiny electronic band gap $\Delta \sim 0.1$ eV acquired—for instance—by elastic strain engineering [54, 55], via substrate-induced superlattices [56, 57] or through Rashba spin splittings on magnetic substrates [58], is perhaps the best suited platform for this purpose. Mainly, because the charge carriers—with mass $m = \Delta/(2v_F^2)$ —in this two dimensional honeycomb lattice of carbon atoms possess a Dirac-like dispersion relation near the neutrality points in which the Fermi velocity $v_F \approx c/300$ plays the role of the speed of light [59]. Hence, their behavior can be effectively described by a $2 + 1$ dimensional Dirac model and their coupling to an electromagnetic field suitably simulates a planar QED with the particularization that the creation of electron-hole pairs in band gapped graphene varieties is predicted to occur at a rate $\mathcal{R}_g \sim \exp[-\pi E_g/E]$ that closely resembles the exponential dependence occurring in the Schwinger mechanism [60, 61]. However, in contrast to E_{cr} , the characteristic electric field in graphene with $\Delta \sim 0.1$ eV, $E_g = \Delta^2/(4ev_F) \sim 10^5$ V/cm is rather easy to access or even overpass, opening in this way an enticing window for emulating the dynamically-assisted vacuum breakdown via Landau-Zener transitions catalyzed by the absorption of photons of a fast-oscillating electric mode [62]. It is worth remarking that graphene flakes with tiny band gaps have also been put forward as toy environments to test intriguing low-dimensional effects in the perturbative nonlinear regime of the Breit-Wheeler-like process [63, 64].

We should stress at this point the substantial efforts devoted to simulate various relativistic processes in graphene layers with gapless band structures [$\Delta = 0$]. See for instance Refs. [65, 66] and references therein. Indeed, the first theoretical Landau-Zener studies in graphene were carried out by considering massless electronic excitations [60, 67–73]. Subsequent measurements of optical radiation—emitted presumably by the recombinations of residual electron-hole pairs produced via the aforementioned mechanism [74] [see also Refs. [75, 76]]—and currents induced by two-cycle laser pulses [77, 78] confirmed the phenomenon. Besides, the detection of the current turned out to be sensitive to the carrier envelope phase of the driving field which facilitates a coherent control of massless electron dynamics and emulates a prediction expected within the Schwinger mechanism [11]. Clearly, similar setups could be implemented to probe

field-induced interband transitions of *massive* quasiparticles stimulated by the absorption of photons of a weak but fast-oscillating wave. As in this scenario the transition rate is enhanced, the yielded electron-hole pairs would have a density higher than in the absence of the weak field, provided $E_g \gg E$. It is then likely that the recombination and so the emission of photons becomes noticeable, or alternatively, that a sizable current can be measured for verifying the first-principle proof of concept of the dynamically-assisted Schwinger mechanism through its described solid-state analog. This paper is devoted to investigate theoretically the latter possibility. To this end, we will adopt a quantum kinetic approach [61], similar to the one which models the pair production process in QED [79–81]. Our effort is oriented toward gaining insights into the amplification that the current undergoes when a strong electric field is active, and quanta from the fast-oscillating wave are absorbed in the meanwhile.

This paper is organized as follows. In Sec. II A, we adopt the model to be analyzed and briefly summarize the main aspects linked to the quantum kinetic equation to be used. In Sec. II B its solution is determined within the low-density approximation by taking the external homogeneous background as a superposition of a strong static electric field and a fast-oscillating electric mode. This analytical approach is also contrasted with the numerical solution of the original transport equation in Sec. II B. A compact asymptotic formula for the current density related to the residual number of excitations is derived in Sec. III A. The established current expression illustrates that the enhancement in conductivity is brought on by the absorption of quanta from the fast-oscillating mode. Later on, in Sec. III B, our study is further extended by considering a full numerical treatment for the current density. In this section, we compare numerical and analytical predictions and identify the parameters that ensure an optimal current due to the photo-catalyzation of Landau-Zener transitions. We conclude the paper in Sec. IV with an overview of our main results.

II. THE QUASIPARTICLE SPECTRUM

A. General aspects

Let us consider the spontaneous production of electron-hole pairs taking place in a time-dependent but homogeneous electric field combining a strong static mode with strength E_s and a perturbative monochromatic wave with amplitude E_w [$E_w \ll E_s$] and frequency ω . Hereafter we will assume both fields localized temporally between $-T/2 \leq t \leq T/2$, so that the pulse length of the wave $T = 2\pi N/\omega$ can be written in terms of the number of cycles N . The corresponding four-potential

reads

$$\mathcal{A}^\mu(t) = b^\mu \begin{cases} +\frac{1}{2}cE_sT & t < -\frac{1}{2}T \\ -cE_s t - \frac{cE_w}{\omega} \sin(\omega t) & -\frac{1}{2}T \leq t \leq \frac{1}{2}T \\ -\frac{1}{2}cE_sT & t > \frac{1}{2}T \end{cases}, \quad (1)$$

where b^μ is the polarization four-vector. In practice, the strong field might result from a capacitor with a dc voltage in which the graphene sheet is placed [see Fig. 1a]. Conversely, a fast-oscillating electric wave can be successfully generated from an incident laser beam with a polarization parallel to the strong field direction. Observe that, to fit with our theoretical treatment, the waist size w_0 of the linearly polarized laser wave has to be much larger than the length of the graphene surface, which we take here of the order of $\ell \gtrsim 100 \mu\text{m}$. The described mechanism does not provide a pure electric wave as it is required by Eq. (1). Indeed, the incident wave—which can be thought as a plane-wave—is not homogeneous and, thus, a magnetic field parallel to the graphene surface would be present. However, the two-dimensional confinement of the quasiparticles prevents any influence of this field component on their dynamics. Hence, what they undergo actually is nothing but the combination of a weak electric field oscillating in time and the strong field linked to the capacitor. Clearly, we may also consider the possibility of another source for the strong field generated from an additional laser beam with a frequency $\Omega \ll \omega$ and intensity higher than the one associated with the fast-oscillating wave. The upcoming study must be then understood in such a situation as the leading order contribution of an adiabatic approximation.

Here, the interband transitions of electrons will be investigated by adopting a quantum kinetic approach. This formulation—which is equivalent to other well-known approaches based on QED in unstable vacuum [1–4]—comprises the dynamical information of the pair production process in the single-quasiparticle distribution function $W_g(\mathbf{p}; t)$, which refers to fixed spin and valley quantum numbers and relaxes to those linked to the electrons and holes only when the total external field is switched off $\mathbf{E}(\pm\infty) \rightarrow 0$, i.e. formally at $t \rightarrow \pm\infty$. In this context, the quantum Boltzmann-Vlasov equation which dictates the time evolution of $W_g(\mathbf{p}; t)$ reads [61, 62, 82, 83]:

$$\begin{aligned} \dot{W}_g(\mathbf{p}; t) = & Q(\mathbf{p}, t) \int_{-\infty}^t dt' Q(\mathbf{p}, t') \left[\frac{1}{2} - W_g(\mathbf{p}; t') \right] \\ & \times \cos \left[2 \int_{t'}^t dt'' w_{\mathbf{p}}(t'') \right], \end{aligned} \quad (2)$$

where the initial condition $W_g(\mathbf{p}, -\infty) = 0$, i.e., an initially empty conduction band is assumed. This formula is characterized by the function $Q(\mathbf{p}, t) \equiv eE(t)v_F \epsilon_{\perp} / w_{\mathbf{p}}^2(t)$, which depends on the quantity $\epsilon_{\perp} = \sqrt{\frac{1}{4}\Delta^2 + p_{\perp}^2 v_F^2}$ and the respective total energy $w_{\mathbf{p}}(t) =$

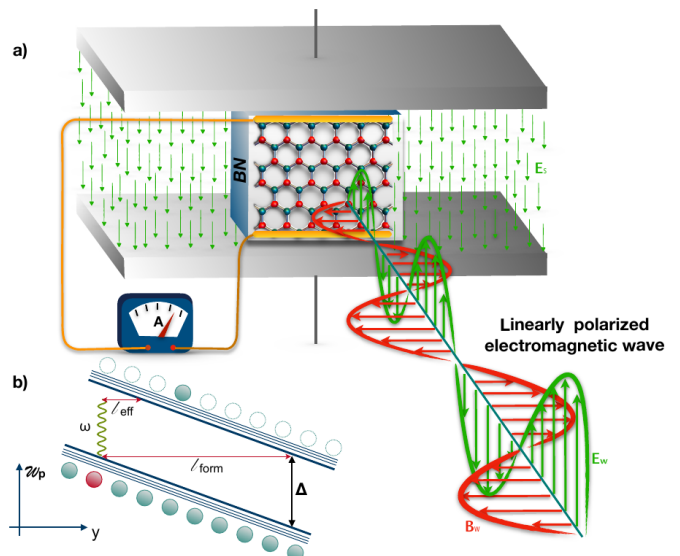


FIG. 1: a) Scheme of an experimental set-up allowing the simulation of the dynamically-assisted Schwinger effect in band-gapped graphene via the production of electron-hole pairs. A graphene flake—grown on top of a substrate—is placed within the plates of a capacitor which holds a strong electric field E_s . Simultaneously, the graphene sheet is irradiated with a linearly polarized plane-wave with frequency ω , the amplitude of which E_w is supposed to be weaker than the field generated by the capacitor [$E_w \ll E_s$]. The field-induced current in the graphene flake is then measured with the help of an ammeter. To this end, two electrodes are deposited on the stripe. b) The tilt that the relativistic-like dispersion relation undergoes owing to the strong electric field makes it possible for electrons—blobs colored in cyan—to tunnel from the valence band to the initially empty conduction band. The absorption of a photon of energy slightly below the band gap [$\omega < \Delta$] reduces the effective distance needed to reach the latter.

$\sqrt{\epsilon_{\perp}^2 + [p_{\parallel} - e\mathcal{A}(t)/c]^2 v_F^2}$. Hereafter, \mathbf{p}_{\perp} and \mathbf{p}_{\parallel} will refer to the components of canonical momentum of the quasiparticle perpendicular and parallel to the direction of the electric field $\mathbf{E}(t) = -\partial\mathcal{A}/\partial(ct) = \mathbf{E}_s + \mathbf{E}_w \cos(\omega t)$ [$\mathcal{A}_0(t) = 0$], respectively. As no dependence on temperature is manifested in Eq. (2), any outcome resulting from it must be interpreted within the zero temperature limit. Therefore, at asymptotically earlier times $t \rightarrow -\infty$ for which both $\mathcal{A}(t)$ and $E(t)$ vanish, the system behaves as a degenerate Fermi gas. In line with this limit, the quasiparticle energy $w_{\mathbf{p}}(-\infty) \rightarrow \sqrt{p^2 v_F^2 + \frac{1}{4}\Delta^2}$ has to be understood relative to the Fermi-level, here assumed at $\epsilon_F = 0$. At this point, it is worth noting that the momentum $\mathbf{p}_{\perp}, \mathbf{p}_{\parallel}$ has to be understood relative to the \mathbf{K} and \mathbf{K}' points and satisfying the condition $|\mathbf{p}| \ll |\mathbf{K}|, |\mathbf{K}'| \approx 3 \text{ eV}/v_F$. Besides, the generation of the gap Δ is conceived here via a substrate-induced mechanism. Indeed, the graphene flake is supposed to be on the surface of hexagonal Boron Nitride (BN), for instance. This implies that, because of the BN dielectric constant $\epsilon_{\text{BN}} \approx 3.4$ [84], the field strength that the graphene sheet

experiences is diminished by a factor of $2/(1+\varepsilon_{\text{BN}}) \approx 0.4$ when compared to the vacuum situation. Consequently, both E_s and E_w are supposed to take this reduction into account.

B. Low-density approximation

Exact solutions of Eq. (2) are known for a few special backgrounds, e.g., constant and Sauter-type electric fields. Beyond these configurations, the problem of finding analytical solutions becomes an intractable task. However, estimates can be obtained by using the low-density approximation [$W_g(\mathbf{p}; t) \ll 1/2$] within the Boltzmann-Vlasov equation. In such a case, the single-quasiparticle distribution function at times, for which the field has been switched off [$W_g(\mathbf{p}) \equiv \lim_{t \rightarrow T/2} W_g(\mathbf{p}; t)$], can be written as [13, 81]

$$W_g(\mathbf{p}) \approx \left| \frac{1}{2} \int_{-T/2}^{T/2} d\tilde{t} Q_{\mathbf{p}}(\tilde{t}) e^{2i \int_0^{\tilde{t}} dt u_{\mathbf{p}}(t)} \right|^2. \quad (3)$$

The term within the absolute value is nothing but one of the Bogoliubov coefficients involved in the problem. After the change of variables $\tau = [p_{\parallel} - e\mathcal{A}(\tilde{t})/c]v_{\text{F}}/\varepsilon_{\perp}$ and $\tilde{\tau} = [p_{\parallel} - e\mathcal{A}(t)/c]v_{\text{F}}/\varepsilon_{\perp}$, the integral in Eq. (3) becomes

$$\int_{-T/2}^{T/2} d\tilde{t} \dots = \int_{\frac{\gamma_{\perp} - \frac{\pi N}{\gamma_{\perp}}}{\gamma_{\perp} + \frac{\pi N}{\gamma_{\perp}}}}^{\frac{\gamma_{\perp} + \frac{\pi N}{\gamma_{\perp}}}{\gamma_{\perp} - \frac{\pi N}{\gamma_{\perp}}}} \frac{d\tau}{1 + \tau^2} \exp \left[\frac{\varepsilon_{\perp}^2}{2eE_s v_{\text{F}}} \mathcal{S}(\tau) \right], \quad (4)$$

$$\mathcal{S}(\tau) = 4i \int_0^{\tau} d\tilde{\tau} \frac{(1 + \tilde{\tau}^2)^{1/2}}{1 + \varepsilon \cos(\omega t)},$$

where

$$\varepsilon = \frac{E_w}{E_s} \ll 1 \quad (5)$$

parametrizes the relative weakness of the fast-oscillating mode. The expression above constitutes the starting point for further considerations. In its second line, t has to be considered as a function of $\tilde{\tau}$. However, this inversion cannot be determined analytically, but only through reversion of the corresponding series [85, 86]. In this case, the leading-order term $t(\tilde{\tau}) \approx (\gamma_{\perp} \tilde{\tau} - \gamma_{\parallel})/\omega$ coincides with the inverse of the function $\tau(t)$ averaged over a cycle of the weak field. Here, we have introduced the dimensionless parameters

$$\gamma_{\parallel} = 2\gamma \frac{p_{\parallel} v_{\text{F}}}{\Delta} \quad \text{and} \quad \gamma_{\perp} = 2\gamma \frac{\varepsilon_{\perp}}{\Delta}. \quad (6)$$

We note that, in the limit of $p_{\perp} \rightarrow 0$, γ_{\perp} reduces to the combined Keldysh parameter [$\gamma = \omega\Delta/(2eE_s v_{\text{F}})$]. In order to suitably simulate the dynamically-assisted Schwinger effect, the band gap Δ has to satisfy simultaneously the conditions $\Delta^2 \gg 4eE_s v_{\text{F}}$ and $\Delta > \omega$. We observe that an assisted scenario with $\Delta > \omega \gtrsim \frac{1}{2}\Delta$

is featured by the restriction $\gamma_{\perp} \geq \gamma \gg 1$. On the contrary, for frequencies $\omega \ll \frac{1}{2}\Delta$ and a strong field $E_s \ll \Delta^2/(4e v_{\text{F}})$, the effective reduction of the barrier width [see Fig. 1b] between the valence and conducting bands $l_{\text{eff}} \sim (\Delta - \omega)/(eE_s)$ approximates to the formation length $l_{\text{form}} \sim \Delta/(eE_s)$ associated with the production of electron-hole pairs when the strong field is present only.

There is a tight parallelism between the process under consideration and the one occurring in a pure QED context. Indeed, structurally, the expressions contained in Eq. (4) resemble those encompassed in Eq. (4) of Ref. [28]. Hence, we can readily adapt the procedure to the problem under consideration and integrate τ approximately via the steepest-descent method.³ As a consequence of this assessment, the Bogoliubov's coefficient which determines $W_g(\mathbf{p})$ approximates

$$\lim_{T \rightarrow \infty} \frac{1}{2} \int_{-T/2}^{T/2} d\tilde{t} \dots \approx -\frac{\pi}{3} e^{\frac{i\varepsilon_{\perp}^2}{2eE_s v_{\text{F}}} \mathcal{S}(i)}, \quad (7)$$

where the expression for $\mathcal{S}(i)$ can be read off from Eq. (4). This formula applies whenever $\varepsilon_{\perp}^2 \gg 2eE_s v_{\text{F}}$ and for times larger than any other characteristic time scale linked to the pair production process. The use of Eq. (7) allows us to approximate the single-quasiparticle distribution function [see Eq. (3)] at asymptotically large time by

$$W_g(\mathbf{p}) \approx e^{-\frac{\varepsilon_{\perp}^2}{\varepsilon E_s v_{\text{F}}} \text{Im } \mathcal{S}(i)}. \quad (8)$$

Here an unessential preexponential factor of the order of unity [$\pi/3 \approx 1.04$] has been omitted. By taking $\tilde{\tau} = iy$, the imaginary parts of $\mathcal{S}(i)$ can be expressed as

$$\text{Im } \mathcal{S}(i) = 4 \int_0^1 dy [1 + \varepsilon \cosh(\gamma_{\perp} y) \cos(\gamma_{\parallel})]$$

$$\times \frac{\sqrt{1 - y^2}}{[1 + \varepsilon \cosh(\gamma_{\perp} y) \cos(\gamma_{\parallel})]^2 + \varepsilon^2 \sinh^2(\gamma_{\perp} y) \sin^2(\gamma_{\parallel})}. \quad (9)$$

The established distribution function $W_g(\mathbf{p})$ [see Eq. (8)] turns out to be a 2π -periodic function in γ_{\parallel} . As it is also even in this variable, the study of its behavior in γ_{\parallel} can be restricted to the region $0 \leq \gamma_{\parallel} \leq \pi$. This translates into $0 \leq p_{\parallel} \leq \pi/\gamma$. We point out that in this interval, $W_g(\mathbf{p})$ decreases monotonically in p_{\parallel} for any p_{\perp} , provided the condition $\gamma_{\perp} \gg \gamma_{\text{cr}}$ is satisfied. Here, the critical Keldysh parameter [22, 26–28, 87]

$$\gamma_{\text{cr}} = \ln \left(\frac{2}{\varepsilon} \right) > 1, \quad \varepsilon \ll 1 \quad (10)$$

defines the crossover between the regime dominated by the absorption of photons from the fast-oscillating wave

³ Readers interested in the chosen integration contour are referred to Ref. [28].

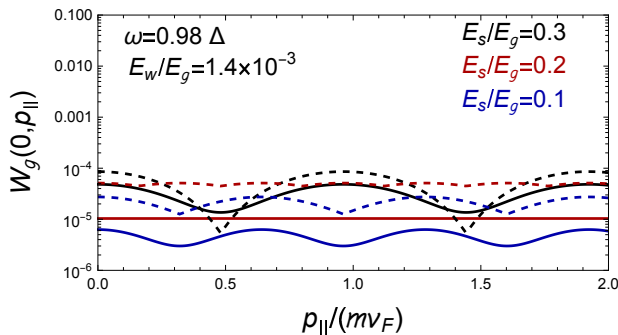


FIG. 2: The long-time behavior of the single-quasiparticle distribution function as a function of the momentum parallel to the external electric field at $p_{\perp} = 0$. For comparison, results from the analytical formula [see Eq. (8)] have been included [dashed curves]. Curves sharing the same color have been obtained by using the same parameters. The numerical outcomes have been obtained by setting the number of cycles $N = 800$, which corresponds to a time $T = 13$ ps if the band gap is chosen as $\Delta = 0.26$ eV. The combined Keldysh parameters $\gamma = 6.5$ for $E_s = 0.3 E_g$, $\gamma = 9.8$ for $E_s = 0.2 E_g$ and $\gamma = 19.6$ for $E_s = 0.1 E_g$, exceed the critical one $\gamma_{\text{cr}} \approx 5$. Here the mass of the carriers is $m = \Delta / (2v_{\text{F}}^2) = 11.7$ keV/ c^2 .

$[\gamma_{\perp} \gg \gamma_{\text{cr}}]$ and the region ruled by the tunneling effect $[\gamma_{\perp} \ll \gamma_{\text{cr}}]$. Indeed, under the former circumstance Eq. (9) behaves as

$$\text{Im } \mathcal{S}(i) \approx 4 \begin{cases} \frac{\gamma_{\text{cr}}}{\gamma_{\perp}} - \frac{1}{\gamma_{\perp}} e^{-\gamma_{\perp}} & \text{for } \gamma_{\parallel} = 0, \\ \frac{\gamma_{\text{cr}}}{\gamma_{\perp}} + \frac{1}{\gamma_{\perp}} e^{-\gamma_{\perp}} & \text{for } \gamma_{\parallel} = \pi. \end{cases} \quad (11)$$

These formulas reveal that, for $p_{\perp} = 0$ and $\gamma \gg \gamma_{\text{cr}}$, the amplitude of oscillations in $W_g(0, p_{\parallel})$ at the extremes of the interval $0 \leq p_{\parallel} \leq \pi/\gamma$ decreases according to the relation

$$\ln [W_g(0, 0)] - \ln [W_g(0, \pi/\gamma)] \sim 4 \frac{\Delta}{\omega} \exp \left[-2 \frac{\omega E_g}{\Delta E_s} \right]. \quad (12)$$

The described features coincide qualitatively with the trends exhibited by the solid curves in Fig. 2, which show the dependence of the single-quasiparticle distribution function on p_{\parallel} when $p_{\perp} = 0$. These outcomes have been obtained by solving numerically the Boltzmann-Vlasov equation [see Eq. (2)]. For this, we transformed it into an equivalent representation described by a system of differential equations [61, 62], and vary $0 \leq p_{\parallel} v_{\text{F}} \leq \Delta$. Furthermore, we have set $\omega = 0.98 \Delta$, $E_w = 1.4 \times 10^{-3} E_g$ and the number of cycles $N = 800$ so that the condition $T \gg |\mathbf{K}| / (eE_s)$ is fulfilled for the three strong field choices $E_s = 0.1 E_g$, $E_s = 0.2 E_g$ and $E_s = 0.3 E_g$. Also in Fig. 2, the corresponding approximated solutions [see Eq. (8)] are depicted in dashed style. Curves sharing the same color have been established using the same set of

parameters. Those in black, for instance, were obtained by setting the strong field to $E_s = 0.3 E_g$, whereas the ones in blue assume $E_s = 0.1 E_g$. While in the former, the approximated result overlaps with the numerical outcome, in the latter, the dashed blue curve qualitatively reproduces the behavior of the corresponding solid one, although its trend along the p_{\parallel} -axis exceeds it by a factor ≤ 5 . A similar deviation is also seen between the approximated and exact numerical patterns, colored in red.

Further insight into the quasiparticle spectrum can be inferred from Fig. 3. There, the behavior of $W_g(\mathbf{p})$ with the momentum perpendicular to the external electric field at $p_{\parallel} = 0$ is depicted. This picture shows clearly that the quasiparticles promoted to the conduction band are more likely to appear at rest. As in Fig. 2, we see that the approximated solutions somewhat differ from the respective numerical outcomes. The exhibited trends suggest that either raising p_{\perp} or decreasing the strong field E_s makes these differences more prominent.

It is worth remarking that, for $\gamma_{\perp} \gg \gamma_{\text{cr}}$, Eq. (11) manifests a significant reduction as compared to the characteristic value linked to the constant field case [$\text{Im } \mathcal{S}(i) \approx \pi$, $W_g(\mathbf{p}) \approx \exp[-\pi \epsilon_{\perp}^2 / (eE_s v_{\text{F}})]$]. As a consequence, the single-quasiparticle distribution function in the photo-catalyzed setup relieves the exponential suppression linked to the case in which $E_w = 0$. Besides, by inserting Eq. (11) into Eq. (8) we end up with

$$W_g(\mathbf{p}) \approx \left(\frac{\epsilon}{2} \right)^{\frac{4\epsilon_{\perp}}{\omega}}, \quad \gamma_{\perp} \gg \gamma_{\text{cr}}. \quad (13)$$

At $\mathbf{p} = 0$, the exponent associated with this asymptotic formula coincides with twice the minimal “number” of quanta necessary to produce a pair at rest from the weak mode solely. This observation already provides evidence that an enhancement in $W_g(\mathbf{p})$ could take place via the absorption of a quantum from the fast-oscillating wave, as compared with the case in which only a constant electric field drives the interband transitions of electrons. To verify this statement, we suppose that the quasiparticles are created in an assisted field setup characterized by the following parameters: $\omega = 0.98 \Delta$ with $\Delta = 0.26$ eV and a critical field $E_g = \Delta^2 / (4e v_{\text{F}}) = 2.6 \times 10^5$ V/cm. If the strong field in the capacitor or the peak field strength of the strong laser is tuned to $E_s = 10^{-1} E_g$, the combined Keldysh parameter $\gamma \approx 19.6$. We note that, if the field strength of the fast-oscillating wave is $E_w = 1.4 \times 10^{-3} E_g$ corresponding to $\epsilon = 1.4 \times 10^{-2}$, the critical Keldysh parameter is $\gamma_{\text{cr}} \approx 5$. Under such circumstances $W_g(\mathbf{0}) \approx 1.9 \times 10^{-4}$ exceeds by 10 orders of magnitude the corresponding distribution function $W_g(\mathbf{0}) \approx 2.3 \times 10^{-14}$ of the standard Landau-Zener process.

Let us consider the case ruled by the condition $\gamma_{\text{cr}} \gg \gamma_{\perp}$. In such a situation all instances in Eq. (9) depending on ϵ can be Taylor expanded. After the integration,

$$W_g(\mathbf{p}) \approx e^{-\frac{\pi \epsilon_{\perp}^2}{e E_s v_{\text{F}}}} \left[1 - \frac{2}{\gamma_{\perp}} \epsilon I_1(\gamma_{\perp} \cos(\gamma_{\parallel})) \right], \quad \gamma_{\text{cr}} \gg \gamma_{\perp}, \quad (14)$$

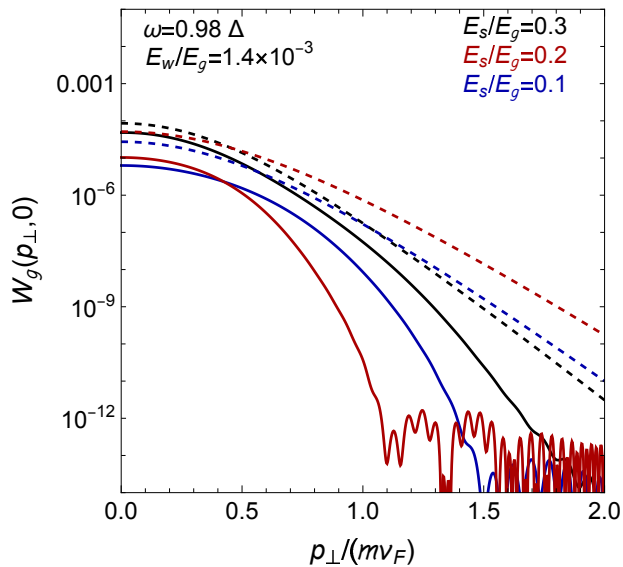


FIG. 3: The long-time behavior of the single-quasiparticle distribution function as a function of the momentum perpendicular to the external electric field at $p_{\parallel} = 0$. We use the same benchmark values and notation as in Fig. 2.

where $I_1(x) = \frac{x}{2} + \frac{x^3}{2^2 4} + \frac{x^5}{2^2 4^2 6} + \dots$ denotes the modified Bessel function of the first kind with order 1 [88]. Also in this limiting case, $W_g(\mathbf{p})$ manifests clearly a monotonic increase in $0 \leq \gamma_{\parallel} \leq \pi$. However, in contrast to the previous case, the amplitude of oscillation in γ_{\parallel} scales as $\sim 2\pi\varepsilon$. Clearly, the distribution function given above reduces to the one associated with a constant electric field when $\varepsilon \rightarrow 0$.

It is worth remarking that, to be consistent with our low-density approximation [see above Eq. (3)], the found distribution function $W_g(\mathbf{p})$ has to remain smaller than $1/2$. This restriction limits the growing of $W_g(\mathbf{p})$ when E_s decreases gradually. Indeed, at $\mathbf{p} = \mathbf{0}$, this condition constrains the field strengths $E_s \gg \frac{1}{2} E_w 2^{\frac{2\omega}{\Delta}}$. Inserting the parameters utilized previously, it will imply that $E_s \gg 2.1 \times 10^{-3} E_g$.

III. RESIDUAL PHOTO-EXCITED CURRENT

The mean current density along the applied electric field direction, induced by the spontaneous creation of electron-hole pairs, splits into two contributions [69, 89]:

$$j(t) = j_{\text{con}}(t) + j_{\text{pol}}(t) \quad (15)$$

identified as the conduction $j_{\text{con}}(t)$ and polarization $j_{\text{pol}}(t)$ currents [90–92]. Explicitly,

$$j_{\text{con}}(t) = 2eg_s g_v \int \frac{d^2 p}{(2\pi)^2} \frac{\partial \mathbf{w}_{\mathbf{p}}(t)}{\partial p_{\parallel}} W_g(\mathbf{p}; t), \quad (16)$$

$$j_{\text{pol}}(t) = 2eg_s g_v \int \frac{d^2 p}{(2\pi)^2} \frac{\mathbf{w}_{\mathbf{p}}(t)}{eE(t)} \dot{W}_g(\mathbf{p}; t).$$

The factor 2 in these expressions is due to the contribution of both the quasiparticles and holes. Here, $g_s = 2$ ($g_v = 2$) accounts for the spin (valley) degeneracy. The formulae above constitute the starting point of further considerations.

A. Behavior of $j(t)$ at asymptotically large times

At times for which the field has been switched off the velocity of the carriers saturates to the Fermi velocity $\lim_{t \rightarrow T/2} \partial \mathbf{w}_{\mathbf{p}}(t) / \partial p_{\parallel} \rightarrow v_F$, provided the condition below Eq. (9) is fulfilled. Under such circumstances the residual current of conduction $j_{\text{con}} \equiv \lim_{t \rightarrow T/2} j_{\text{con}}(t)$ approximates $j_{\text{con}} \approx 2e v_F \mathcal{N}_g$, with \mathcal{N}_g referring to the density of electrons that occupies the initially empty upper Dirac cone

$$\mathcal{N}_g = g_s g_v \int \frac{d^2 p}{(2\pi)^2} W_g(\mathbf{p}). \quad (17)$$

This constitutes an evidence that $j_{\text{con}}(t)$ is indeed caused by the motion of the produced carriers. Now, the vacuum breakdown is accompanied by the production of electric dipoles linked to each electron-hole pair which is created. In a semi-classical picture, this dipole moment becomes separated by an instantaneous barrier width $\ell_{\text{eff}}(t) = 2\mathbf{w}_{\mathbf{p}}(t)/[eE(t)]$ and has a magnitude $\mathbf{p}(t) = 2e\ell_{\text{eff}}(t)$. The polarization current is therefore caused by the rate at which these dipoles are created. Observe that, at a time for which the electric field has been switched off, the dipole is $\lim_{t \rightarrow T/2} \mathbf{p}(t) = 2eT v_F$ and $j_{\text{pol}} \equiv \lim_{t \rightarrow T/2} j_{\text{pol}}(t) \approx e v_F T \dot{\mathcal{N}}_g$. It is worth remarking that $\lim_{t \rightarrow T/2} \dot{W}_g(\mathbf{p}, t) \propto Q(\mathbf{p}, T/2) \approx 4\gamma_{\perp}/(\omega T^2)$, provided the condition $T \gg 2|p_{\perp, \parallel}|/(eE_s)$ applies [see Eq. (2) and below Eq. (9)]. As a result, the residual polarization current $j_{\text{pol}} \propto T^{-1}$ is suppressed at asymptotically large times. It can, thus, be safely ignored in our calculation and Eq. (15) approximates

$$j \approx 2e v_F \mathcal{N}_g. \quad (18)$$

To be consistent with both the application range of the Dirac model [see discussion below Eq. (2)] and the condition under which $W_g(\mathbf{p})$ was derived [see below Eq. (9)], the integration domains have to be limited by the $\min\{|\mathbf{K}|, \frac{1}{2}eE_s T\}$. In what follows, we shall consider the field regime in which its finite extension has no impact on the interband transitions of electrons, i.e., $|\mathbf{K}| \ll \frac{1}{2}eE_s T$. Hence, we use $-|\mathbf{K}| \leq p_{\perp, \parallel} \leq |\mathbf{K}|$ when computing the two-dimensional integration numerically. However, from an analytical prospect, the fast damping of the integrand in both $p_{\perp, \parallel}$ allows us to extend the corresponding integration limits to $\pm\infty$ without introducing an appreciable error. Considering the periodicity of $W_g(\mathbf{p})$ in p_{\parallel} , as well as its even character in both p_{\parallel} and

p_{\perp} we find that the density of created pairs approximates

$$\begin{aligned} \mathcal{N}_g &\approx g_s g_v |\mathbf{K}| \frac{eE_s}{\pi^3 \omega} \int_0^{\pi} d\gamma_{\parallel} \int_{\gamma}^{\infty} ds \\ &\times \frac{s}{\sqrt{s^2 - \gamma^2}} \exp \left[-\frac{eE_s v_F}{\omega^2} s^2 \text{Im} \mathcal{S}(i; s, \gamma_{\parallel}) \right], \end{aligned} \quad (19)$$

where—after substituting Eq. (8)—the changes of variables $\gamma_{\parallel} = \omega p_{\parallel} / eE_s$ and $s^2 = \omega^2 \epsilon_{\perp}^2 / (eE_s)^2$ have been carried out. The main contribution to the integral over s results from the region close to the singularity, i.e. for $s \sim \gamma$. In the vicinity of γ , the preexponential factor in the integrand behaves approximately as $\gamma^{1/2} / [2(s - \gamma)]^{1/2}$, while the exponent can be expanded around $s \sim \gamma$. We note that to guarantee the convergence of the integral over s , the exponent has to be expanded at least up to linear order. Under this circumstance the variable s can be integrated out. The resulting expression involves an exponent $\text{Im} \mathcal{S}(i; \gamma, \gamma_{\parallel})$. As this function grows monotonically in $[0, \pi]$, the main contribution to the integration over γ_{\parallel} results from the region of γ_{\parallel} for which the exponential suppression is minimized [$\gamma_{\parallel} \sim 0$]. When setting this value in the preexponent and expanding $\text{Im} \mathcal{S}(i; \gamma, \gamma_{\parallel})$ up to γ_{\parallel}^2 , we end up with

$$\begin{aligned} \mathcal{N}_g &\approx g_s g_v |\mathbf{K}| \frac{(eE_s)^{1/2}}{4\pi^{5/2} v_F^{1/2}} \frac{\text{erf} \left(\sqrt{\frac{1}{4} \frac{\Delta}{\omega} \hbar_{\varepsilon}(\gamma) \pi} \right)}{\sqrt{1 - \mathcal{G}_{\varepsilon}(\gamma) - \frac{1}{2} \gamma \mathcal{G}'_{\varepsilon}(\gamma)}} \\ &\times \frac{1}{\sqrt{\frac{1}{4} \frac{\Delta}{\omega} \hbar_{\varepsilon}(\gamma)}} \exp \left[-\pi \frac{E_g}{E_s} \{1 - \mathcal{G}_{\varepsilon}(\gamma)\} \right], \end{aligned} \quad (20)$$

where $\text{erf}(x) = \frac{2}{\sqrt{\pi}} \int_0^x dt e^{-t^2}$ denotes the error function [88]. As we will see shortly, the expression above constitutes an upper limit for the number of created pairs per unit area and applies under the condition $2|\mathbf{K}| \ll eE_s T$. Notice that Eq. (20) contains the functions $\mathcal{G}_{\varepsilon}(\gamma) = 1 - \frac{1}{\pi} \text{Im} \mathcal{S}(i; \gamma, 0)$ and $\mathcal{G}'_{\varepsilon}(\gamma) \equiv \partial \mathcal{G}_{\varepsilon}(s) / \partial s|_{s=\gamma}$ with

$$\mathcal{G}_{\varepsilon}(\gamma) \approx \begin{cases} \frac{2\varepsilon}{\gamma} I_1(\gamma) & \text{for } \gamma \ll \gamma_{\text{cr}}, \\ 1 - \frac{4}{\pi} \frac{\gamma_{\text{cr}}}{\gamma} & \text{for } \gamma \gg \gamma_{\text{cr}} \end{cases} \quad (21)$$

characterizing the decrement of the exponential function. Additionally, Eq. (20) introduces the function $\hbar_{\varepsilon}(\gamma) \equiv \gamma \partial^2 \text{Im} \mathcal{S}(i; \gamma, \gamma_{\parallel}) / \partial \gamma_{\parallel}^2|_{\gamma_{\parallel}=0}$ which remains below unity [$\hbar_{\varepsilon}(\gamma) < 1$] and its asymptotes turn out to be⁴

$$\hbar_{\varepsilon}(\gamma) \approx \begin{cases} 2\pi\varepsilon I_1(\gamma) & \text{for } \gamma \ll \gamma_{\text{cr}}, \\ 4 \frac{\gamma_{\text{cr}}}{\gamma^2} & \text{for } \gamma \gg \gamma_{\text{cr}}. \end{cases} \quad (22)$$

In the regime characterized by the conditions $\gamma \ll 1$ and $\frac{1}{2}\Delta < \omega \lesssim \Delta$, the argument of the error function is

very small and its leading order contribution behaves as $\text{erf}(x) \sim 2x/\sqrt{\pi}$. In such a scenario, Eq. (20) reproduces the expression obtained in Refs. [60, 61]

$$\mathcal{N}_g \approx g_s g_v |\mathbf{K}| \frac{(eE_s)^{1/2}}{2\pi^2 v_F^{1/2}} \exp \left[-\pi \frac{E_g}{E_s} \right]. \quad (23)$$

When $\gamma \gg \gamma_{\text{cr}}$ with $\frac{1}{2}\Delta < \omega \lesssim \Delta$, the small-argument behavior of the error function can still be applied to Eq. (20) and the density $\mathcal{N}_g \propto \varepsilon \frac{2\Delta}{\omega}$. In the intermediate regime not covered by these asymptotic cases, the density rate for pair-production [see Eq. (20)] mixes both tunneling and multiphoton effects. We remark that the formulae linked to the case in which $\frac{1}{2}eE_s T \ll |\mathbf{K}|$ can be read off from Eqs. (20)-(23) via the replacement $|\mathbf{K}| \rightarrow \frac{1}{2}eE_s T$. Clearly, in such a case, the density of electron-hole pairs \mathcal{N}_g scales linearly with the time T . Besides, in the corresponding tunneling regime [$\gamma \ll 1$] the preexponent of \mathcal{N}_g would scale with the well established $(eE_s)^{3/2}$ factor associated with a 2+1 dimensional theory.

B. Numerical results and discussion

In order to assess the enhancement induced by the fast-oscillating wave as compared to the standard Landau-Zener scenario [dotted gray style], we show in Fig. 4 [solid curves] the dependence of j with respect to the strong electric field strength E_s within the range $E_s \in [0.01, 0.4] E_g$ with $E_g = \Delta^2 / (4e v_F)$ the critical field in graphene. We have chosen a gap $\Delta = 0.26$ eV and a number of cycles $N = 2500$ as reference values for our assessment, leading to the characteristic field scale $E_g \approx 2.6 \times 10^5$ V/cm and interaction time $T \approx 21$ ps for $\omega = 0.98 \Delta$, $T \approx 23$ ps for $\omega = 0.88 \Delta$, $T \approx 26$ ps for $\omega = 0.78 \Delta$, and $T \approx 35$ ps for $\omega = 0.58 \Delta$ respectively. In both panels, the parameters used for solid, dotted and dashed curves sharing color are the same. While the plot markers indicate the numerically computed values of the current density, the dashed curves have been obtained from Eq. (18) with \mathcal{N}_g given in Eq. (20). In accordance with the discussion at the end of Sec. II B, the results related to this approximation are exhibited from $E_s \gtrsim 0.1 E_g$. These dashed curves reproduce the numerical patterns qualitatively in this range, with an accuracy that increases as the strong field grows. We remark that each approximated result exceeds the corresponding numerical outcome by a factor close to 5 when $E_s \approx 0.15 E_g$. We have numerically confirmed that the polarization current in the domain under consideration is insignificant compared to the corresponding conduction current. Hence, the difference between the analytical and numerical results can be attributed to the approximations that the analytical expression for the distribution function [see Eq. (8)] relies on.

The current in both panels has a pronounced nonlinear dependence on E_s , which is related to a dc conductivity

⁴ For further details we refer the reader to Ref. [28].

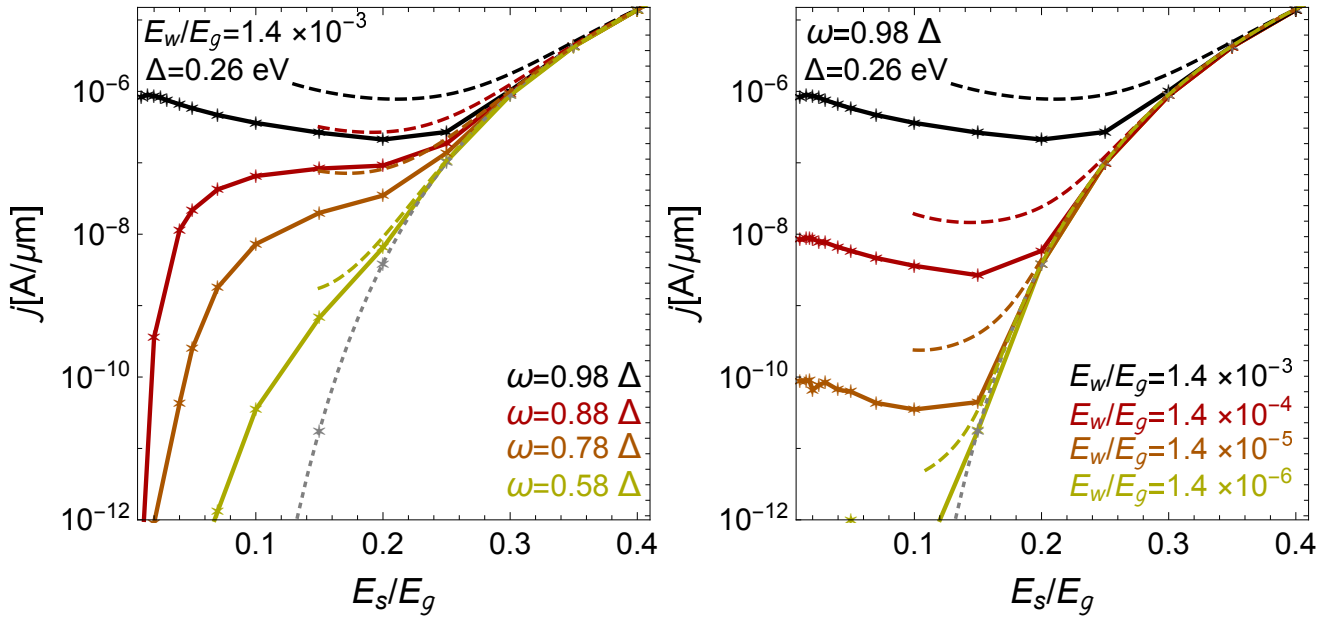


FIG. 4: Current density at the stage in which the field configuration is turned off. In both panels, the plot markers indicate the numerically computed values which have been obtained by setting $N = 2500$ and by limiting the two-dimensional integration to the region $-|\mathbf{K}| \leq p_{\perp, \parallel} \leq |\mathbf{K}|$. For comparisons, the outcomes resulting from the analytical formula have been included [dashed curves]. In each panel, curves sharing the same color have been obtained by using the same parameters. The dotted curve in gray results from the standard Landau-Zener mechanism, i.e., for $E_w = 0$. All curves have been generated by using a gap $\Delta = 0.26$ eV leading to a critical field $E_g = \Delta^2/(4ev_F) \approx 2.6 \times 10^5$ V/cm.

that is field-dependent. An approximated expression for this quantity can be inferred by comparing Eq. (18) with Ohm's law [$j = \sigma E_s$] and reads

$$\sigma \approx e^2 \frac{g_s g_v |\mathbf{K}| v_F^{1/2}}{2\pi^{5/2} (eE_s)^{1/2}} \frac{\text{erf}\left(\sqrt{\frac{1}{4} \frac{\Delta}{\omega} \hbar \epsilon(\gamma) \pi}\right)}{\sqrt{1 - g_\epsilon(\gamma) - \frac{1}{2} \gamma g'_\epsilon(\gamma)}} \times \frac{1}{\sqrt{\frac{1}{4} \frac{\Delta}{\omega} \hbar \epsilon(\gamma)}} \exp\left[-\pi \frac{E_g}{E_s} \{1 - g_\epsilon(\gamma)\}\right], \quad (24)$$

where Eq. (20) has been used.

The results shown in the left panel have been obtained by setting the weak field strength to $E_w = 1.4 \times 10^{-3} E_g$. Each solid curve there is linked to a particular laser frequency, and as this parameter increases, it becomes clear that the results differ significantly from the ones associated with the standard Landau-Zener transitions [dotted gray style]. This enhancement is attributed to the absorption of photons from the fast-oscillating wave in the presence of the strong field, and it becomes particularly noticeable in the range of E_s exhibited in Fig. 4. It is confirmed on both panels that there are two paths to boost the interband transitions of electrons in a photocatalyzed system. Namely, by strengthening the strong field or through absorption of quanta from the fast-oscillating beam. The former channel rules the process as E_s increases, while the latter dominates as the contrary condition occurs. It is worth noting that for frequencies $\omega \approx 0.98 \Delta$, the curves tend to exhibit a local maximum

at $E_s \approx 1.5 \times 10^{-2} E_g$. Indeed, for this parameter combination the current amounts to $j_{\text{max}} \approx 9 \times 10^{-7}$ A/ μm . The emergence of this local maximum is a remarkable feature that would allow us to verify the process with a field strength E_s which is two orders of magnitude weaker than E_g .⁵

In contrast to the left panel, the right panel is intended to provide insight about the trend of the current density with the change of E_w . There, the curves have been obtained by setting the laser frequency to $\omega = 0.98 \Delta$. Certainly, the revealed outcomes closely mirror those patterns that have been predicted in a pure QED context for the number of electron-positron pairs to be produced in a dynamically-assisted scenario [see the left panel of Fig. 5 in Ref. [28]]. At this point it is worth mentioning that the information depicted in Fig. 4 can be transferred to the yielded density of electron-hole pairs as well because $j \sim \mathcal{N}_g$. We note that, as the fast-oscillating wave becomes weaker, all solid curves in this panel tend to stick closer to the one linked to the standard Landau-Zener

⁵ If this result is extrapolated to a pure QED context, it would suggest that a standing wave, made out from the collision of two energetic photon sources with frequency $\omega = 1.96 m_e c^2$ and intensity $I_w \sim 10^{23}$ W/cm² is required alongside with another strong standing wave that results from the collision of two optical laser fields—frequency $\Omega = \mathcal{O}(1)$ eV—with a peak intensity of $I_s \sim 10^{25}$ W/cm². None of the required laser fields are currently available.

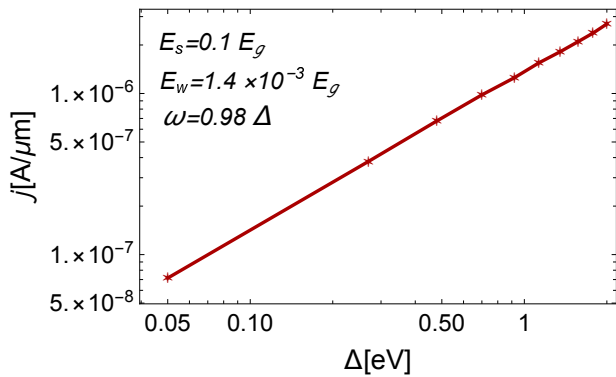


FIG. 5: Current density as a function of the gap parameter in the assisted field configuration’s turning off stage. The benchmark parameters and notation used in Fig. 4 have also been adopted here.

current. Besides, one can learn more about how the current density scales with the weak field E_w by comparing plot markers of various curves at a fixed E_s . For instance, at $E_s = 0.1 E_g$ one could naively conclude that j scales linearly with E_w . However, the spacing between plot markers reduces substantially as they approximate the gray dotted curve. This is clearly seen at $E_s = 0.15 E_g$, and reveals that the dependence on E_w is not linear in general. The findings exhibited in the right panel also suggest that the weak field’s variation slightly modifies the location of the maximum.

Let us estimate the current $\mathcal{I} = j\ell$ to be measured by sending a single laser shot through the setup of Fig. 1a. To this end we consider graphene samples with length $\ell \gtrsim 100 \mu\text{m}$. In order to put our outcomes in context, we shall refer to an experiment in which optimal conditions are achieved. Hence, we will suppose a strong field $E_s = 0.015 E_g = 3.9 \times 10^3 \text{ V/cm}$. Under such a circumstance the current density due to standard Landau-Zener transitions is vanishingly small, $j_{LZ} \sim 10^{-97} \text{ A}/\mu\text{m}$. Next, let us suppose that a fast-oscillating wave with frequency $\omega = 0.98 \Delta \approx 0.25 \text{ eV}$ [$\lambda \approx 4.8 \mu\text{m}$] and peak intensity $I_w = c(1 + \varepsilon_{\text{BN}})E_w^2/2 \approx 8.8 \times 10^2 \text{ W/cm}^2$ —corresponding to $E_w = 1.4 \times 10^{-3} E_g = 3.6 \times 10^2 \text{ V/cm}$ —irradiates the graphene flake while the preceding strong field is switched on. According to the results in Fig. 4, the corresponding current density $j_{\text{max}} \approx 9 \times 10^{-7} \text{ A}/\mu\text{m}$ [see solid black curve] turns out to be many orders of magnitude larger than j_{LZ} and corresponds to a measurable current of $\mathcal{I} = j\ell \gtrsim 90 \mu\text{A}$ at the stage in which the assisted field configuration is turned off. Noteworthy, this prediction could be measurable with presently available technology. Indeed, in graphene layers with gapless band structures [$\Delta = 0$], photo-excited currents $\sim \text{pA}$ have already been detected via Landau-Zener-Stückelberg interferometry [77, 78]. To assess the extent to which our estimation depends on the band gap, we show in Fig. 5 the behavior of the current density when Δ varies, while conditions guaranteeing the aforementioned enhancement are held. This result provides evidence that j increases linearly

with the band gap. Hence, the analyzed setup can benefit by setting $\Delta > 0.26 \text{ eV}$.

Let us finish by making a short note about the availability of laser fields to meet characteristics that correspond to those employed in our calculations. In this sense, we find it convenient to remark that our predictions strongly depend on the fulfillment of the condition $eE_s T \gg 2|\mathbf{K}|$, implying that the field configuration has to be active for a time longer than 16 ps for $E_s = 0.015 E_g$, for instance. This constraint, as well as others that have emerged during the calculations—read the beginning of this section—can be easily satisfied with nanosecond lasers with tunable wavelengths [see, for instance, the class available at [93]]. We note that, for graphene samples with length $\ell \gtrsim 100 \mu\text{m}$, the ballistic flight time $t_{\text{ball}} \approx \ell v_F^{-1} \gtrsim 0.1 \text{ ns}$ is comparable with the pulse length of some of these lasers.

IV. CONCLUSIONS

We have investigated how the interband transitions of electrons caused by a strong static electric field are highly stimulated by the absorption of photons with energies slightly below the gap of semiconductor graphene flakes. Our study has been based on the Dirac-like model, which allows us to incorporate naturally some fundamental principles of quantum electrodynamics and, likewise, to adopt an out-of-equilibrium quantum field theory description for the process. We have established important features, including conditions that would ensure its optimization, and pointed out that measurements of the generated current can serve as a first-principle-proof of concept of the dynamically-assisted Schwinger mechanism in QED. It has been shown, in particular, that the quasiparticle spectrum exhibits evanescent oscillations in the external field’s direction, whereas perpendicular to it, the spectrum diminishes considerably more slowly than in the conventional Landau-Zener process when p_{\perp} increases. A considerable increase in the graphene’s conductivity along the field axis has been predicted, involving nonlinear dependencies on both the strong and weak field strengths. The phenomenon examined here offers a practical method for injecting free-of-contact ultrafast currents with subcritical fields and for controlling the conductivity of the material by adjusting the fast-oscillating laser wave’s parameters.

Acknowledgments

RE acknowledges funding by the Deutsche Forschungsgemeinschaft (DFG, German Research Foundation), under Projektnummer 277101999 – TRR 183 (project B04), and under Germany’s Excellence Strategy – Cluster of Excellence Matter and Light for Quantum Computing (ML4Q) EXC 2004/1 – 390534769.

-
- [1] D. M. Gitman, Processes of arbitrary order in quantum electrodynamics with a pair-creating external field, *J. Phys. A* **10**, 2007 (1977).
- [2] E. S. Fradkin, D. M. Gitman, and S. M. Shvartsman, *Quantum Electrodynamics with Unstable Vacuum* Springer-Verlag, Berlin, (1991).
- [3] S. P. Grivilov and D. M. Gitman, Vacuum instability in external fields, *Phys. Rev. D* **53**, 7162 (1996).
- [4] S. P. Grivilov and D. M. Gitman, Vacuum instability in slowly varying electric fields, *Phys. Rev. D* **95**, 076013 (2017).
- [5] F. Sauter, Über das Verhalten eines Elektrons im homogenen elektrischen Feld nach der relativistischen Theorie Diracs, *Z. Phys.* **69**, 742 (1931).
- [6] W. Heisenberg and H. Euler, Folgerungen aus der Diracschen Theorie des Positrons, *Z. Phys.* **98**, 714 (1936).
- [7] J. S. Schwinger, On gauge invariance and vacuum polarization, *Phys. Rev.* **82**, 664 (1951).
- [8] See: <http://www.eli-laser.eu>
- [9] See: <http://xcels.iapras.ru/>
- [10] R. Alkofer, M. B. Hecht, C. D. Roberts, S. M. Schmidt and D. V. Vinnik, Pair creation and an X-ray free electron laser, *Phys. Rev. Lett.* **87**, 193902 (2001).
- [11] F. Hebenstreit, R. Alkofer, G. Dunne and H. Gies, Momentum signatures for Schwinger pair production in short laser pulses with sub-cycle structure, *Phys. Rev. Lett.* **102**, 150404 (2009).
- [12] S. S. Bulanov, V. D. Mur, N. V. Narozhny, J. Nees, and V. S. Popov, Multiple Colliding Electromagnetic Pulses: A Way to Lower the Threshold of positron and electron Pair Production from Vacuum, *Phys. Rev. Lett.* **104**, 220404 (2010).
- [13] D. B. Blaschke, B. Kämpfer, A. D. Panferov, A. V. Prozorkevich, and S. A. Smolyansky, Influence of laser pulse parameters on the properties of e^-e^+ plasma created from vacuum, *Contrib. Plasma Phys.* **53**, 165 (2013).
- [14] C. Kohlfürst, M. Mitter, G. von Winckel, F. Hebenstreit, and R. Alkofer, Optimizing the pulse shape for Schwinger pair production, *Phys. Rev. D* **88**, 045028 (2013).
- [15] A. Gonoskov, I. Gonoskov, C. Harvey, A. Ilderton, A. Kim, M. Marklund, G. Mourou, and A. Sergeev, Probing Nonperturbative QED with Optimally Focused Laser Pulses, *Phys. Rev. Lett.* **111**, 060404 (2013).
- [16] F. Hebenstreit, and F. Fillion-Gourdeau, Optimization of Schwinger pair production in colliding laser pulses, *Phys. Lett. B* **739**, 189 (2014).
- [17] C. Banerjee, M. P. Singh, and A. M. Fedotov, Phase control of Schwinger pair production by colliding laser pulses, *Phys. Rev. A* **98**, 032121 (2018).
- [18] R. Schützhold, H. Gies and G. Dunne, Dynamically assisted Schwinger mechanism, *Phys. Rev. Lett* **101**, 130404 (2008).
- [19] G. Dunne, H. Gies and R. Schützhold, Catalysis of Schwinger vacuum pair production, *Phys. Rev. D* **80**, 111301 (2009).
- [20] A. Monin and M. B. Voloshin, Semiclassical calculation of photon-stimulated Schwinger pair creation, *Phys. Rev. D* **81**, 025001 (2010).
- [21] M. Jiang, W. Su, Z. Q. Lv, X. Lu, Y. J. Li, R. Grobe, and Q. Su, Pair creation enhancement due to combined external fields, *Phys. Rev. A* **85**, 033408 (2012).
- [22] M. F. Linder, C. Schneider, J. Sicking, N. Szpak, and R. Schützhold, Pulse shape dependence in the dynamically assisted Sauter-Schwinger effect, *Phys. Rev. D* **92**, 085009 (2015).
- [23] C. Schneider and R. Schützhold, Prefactor in the dynamically assisted Sauter-Schwinger effect, *Phys. Rev. D* **94**, 085015 (2016).
- [24] G. Torgrimsson, J. Oertel, and R. Schützhold, Doubly assisted Sauter-Schwinger effect, *Phys. Rev. D* **94**, 065035 (2016).
- [25] X. G. Huang and H. Taya, Spin-dependent dynamically assisted Schwinger mechanism, *Phys. Rev. D* **100**, 016013 (2019).
- [26] G. Torgrimsson, C. Schneider, J. Oertel, and R. Schützhold, Dynamically assisted Sauter-Schwinger effect – non-perturbative versus perturbative aspects, *J. High Energy Phys.* **06**, 043 (2017).
- [27] G. Torgrimsson, Perturbative methods for assisted non-perturbative pair production, *Phys. Rev. D* **99**, 096002 (2019).
- [28] S. Villalba-Chávez and C. Müller, Signatures of the Schwinger mechanism assisted by a fast-oscillating electric field, *Phys. Rev. D* **100**, 116018 (2019).
- [29] M. Orthaber, F. Hebenstreit, and R. Alkofer, Momentum spectra for dynamically assisted Schwinger pair production, *Phys. Lett. B* **698**, 80 (2011).
- [30] C. Fey, and R. Schützhold, Momentum dependence in the dynamically assisted Sauter-Schwinger effect, *Phys. Rev. D* **85**, 025004 (2012).
- [31] I. Akal, S. Villalba-Chávez and C. Müller, Electron-positron pair production in a bifrequent oscillating electric field, *Phys. Rev. D* **90**, 113004 (2014).
- [32] A. Otto, D. Seipt, D. Blaschke, S. A. Smolyansky, and B. Kämpfer, Dynamical Schwinger process in a bifrequent electric field of finite duration: survey on amplification, *Phys. Rev. D* **91**, 105018 (2015).
- [33] A. Otto, D. Seipt, D. Blaschke, B. Kämpfer, and S. A. Smolyansky, Lifting shell structures in the dynamically assisted Schwinger effect in periodic fields, *Phys. Lett. B* **740**, 335 (2015).
- [34] A. D. Panferov, S. A. Smolyansky, A. Otto, B. Kämpfer, D. B. Blaschke, and L. Juchnowski, Assisted dynamical Schwinger effect: pair production in a pulsed bifrequent field, *Eur. Phys. J. D* **70**, 56 (2016).
- [35] A. Otto, H. Oppitz, and B. Kämpfer, Assisted Vacuum Decay by Time Dependent Electric Fields, *Eur. Phys. J. A* **54**, 23 (2018).
- [36] I. A. Aleksandrov, G. Plunien, and V. M. Shabaev, Dynamically assisted Schwinger effect beyond the spatially-uniform-field approximation, *Phys. Rev. D* **97**, 116001 (2018).
- [37] I. Sitiwaldi and B. S. Xie, Pair production by three fields dynamically assisted Schwinger process, *Phys. Lett. B* **777**, 406 (2018).
- [38] I. Taya, Franz-Keldysh effect in strong-field QED, *Phys. Rev. D* **99**, 056006 (2019).
- [39] A. Di Piazza, E. Lötstedt, A. I. Milstein, and C. H. Keitel, Barrier control in tunneling $e^+ - e^-$ photoproduction, *Phys. Rev. Lett.* **103**, 170403 (2009).
- [40] S. Augustin and C. Müller, Nonperturbative Bethe-Heitler pair creation in combined high- and low- fre-

- quency laser fields, Phys. Lett. B **737**, 114 (2014).
- [41] M. J. A. Jansen and C. Müller, Strongly enhanced pair production in combined high- and low- frequency laser fields, Phys. Rev. A **88**, 052125 (2013).
- [42] D. L. Burke et al., Positron production in multiphoton light-by-light scattering, Phys. Rev. Lett. **79**, 1626 (1997).
- [43] S. Meuren, Probing strong-field QED at FACET-II (SLAC E-320), <https://conf.slac.stanford.edu/facet-2-2019/sites/facet-2-2019.conf.slac.stanford.edu/files//basic-page-docs/sfqed2019.pdf>.
- [44] H. Abramowicz et al., Letter of Intent for the LUXE Experiment, *arXiv:1909.00860*.
- [45] H. Abramowicz et al., *Conceptual design report for the LUXE experiment*, Eur. Phys. J. Spec. Top. **230**, 2445, (2021).
- [46] C. H. Keitel et al., Photo-induced pair production and strong field QED on Gemini, *arXiv:2103.06.059*.
- [47] F. C. Salgado et al., Towards pair production in the non-perturbative regime, New J. Phys. **21**, 105002, (2021).
- [48] A. Golub, S. Villalba-Chávez and C. Müller, Non-linear Breit-Wheeler pair production in collisions of bremsstrahlung γ -quanta and a tightly focussed laser pulse, Phys. Rev. D **105**, 116016 (2022).
- [49] L. Landau, Zur Theorie der Energieübertragung. II, Physik. Z. Sowjet. **2**, 46 (1932).
- [50] C. Zener, Non-Adiabatic Crossing of Energy Levels, Proc. R. Soc. (London) **A137**, 696 (1932).
- [51] K. S. Novoselov, et al., Electric Field effect in atomically thin Carbon films, Science **306**, 666 (2004).
- [52] K. S. Novoselov et al., Two-dimensional atomic crystals, Proc. Natl. Acad. Sci. **102**, 10451 (2005).
- [53] K. S. Novoselov et al., Two-dimensional gas of massless Dirac fermions in graphene, Nature **438**, 197 (2005).
- [54] M. A. H. Vozmediano, M. I. Katsnelson and F. Guinea, Gauge fields in graphene, Phys. Rep. **496**, 109 (2010).
- [55] D. N. Basov, M. M. Fogler, A. Lanzara, F. Wang and Y. Zhang, Colloquium: Graphene Spectroscopy, Rev. Mod. Phys. **86**, 959 (2014).
- [56] S. Y. Zhou et al., Substrate-induced bandgap opening in epitaxial graphene, Nature Materials **6**, 770 (2007).
- [57] G. Giovannetti, P. A. Khomyakov, G. Brocks, P. J. Kelly and J. van den Brink, Substrate-induced band gap in graphene on hexagonal boron nitride: Ab initio density functional calculations, Phys. Rev. B **76**, 073103 (2007).
- [58] A. Varykhalov, J. Sánchez-Barriga, A. M. Shikin, C. Biswas, E. Vescovo, A. Rybkin, D. Marchenko and O. Rader, Electronic and Magnetic Properties of Quasifreestanding Graphene on Ni, Phys. Rev. Lett. **101**, 157601 (2008).
- [59] P. R. Wallace, The band theory of graphite, Phys. Rev. **71**, 622 (1947).
- [60] G. L. Klimchitskaya, and V. M. Mostepanenko, Creation of quasiparticles in graphene by a time-dependent electric field, Phys. Rev. D **87**, 125011 (2013).
- [61] I. Akal, R. Egger, C. Müller and S. Villalba-Chávez, Low-dimensional approach to pair production in an oscillating electric field: Application to bandgap graphene layers, Phys. Rev. D **93**, 116006 (2016).
- [62] I. Akal, R. Egger, C. Müller and S. Villalba-Chávez, Simulating dynamically assisted production of Dirac pairs in gapped graphene monolayers, Phys. Rev. D **99**, 016025 (2019).
- [63] A. Golub, R. Egger, C. Müller and S. Villalba-Chávez, Dimensionality-driven photoproduction of massive Dirac pairs near threshold in gapped graphene monolayers, Phys. Rev. Lett. **124**, 110403 (2020).
- [64] A. Golub, S. Villalba-Chávez and C. Müller, Strong-field Breit-Wheeler pair production in QED₂₊₁, Phys. Rev. D **103**, 096002 (2021).
- [65] A. H. Castro Neto, F. Guinea, N. M. R. Peres, K. S. Novoselov and A. K. Geim, The electronic properties of graphene, Rev. Mod. Phys. **81**, 109 (2009).
- [66] V. N. Kotov, B. U. Uchoa, V. M. Pereira, F. Guinea and A. H. Castro Neto, Electron-electron interactions in graphene: Current Status and Perspectives, Rev. Mod. Phys. **84**, 1067 (2012).
- [67] D. Allor, T. D. Cohen and D. A. McGady, The Schwinger mechanism and graphene, Phys. Rev. D **78**, 096009 (2008).
- [68] M. Lewkowicz and B. Rosenstein, Dynamics of Particle-Hole Pair Creation in Graphene, Phys. Rev. Lett. **102**, 106802 (2009).
- [69] B. Dóra and R. Moessner, Nonlinear electric transport in graphene: Quantum quench dynamics and the Schwinger mechanism, Phys. Rev. B **81**, 165431 (2010).
- [70] M. Lewkowicz, H. C. Kao and B. Rosenstein, Signature of the Schwinger pair creation rate via radiation generated in graphene by a strong electric current Phys. Rev. B. **84**, 035414 (2011).
- [71] H. K. Avetissian, A. K. Avetissian, G. F. Mkrtchian and Kh. V. Sedrakian, Creation of particle-hole superposition states in graphene at multiphoton resonant excitation by laser radiation, Phys. Rev. B **85**, 115443 (2012).
- [72] F. Fillion-Gourdeau and S. MacLean, Time-dependent pair creation and the Schwinger mechanism in graphene, Phys. Rev. B **92**, 035401 (2015).
- [73] F. Fillion-Gourdeau, D. Gagnon, C. Lefebvre and S. MacLean, Time-domain quantum interference in graphene, Phys. Rev. B **94**, 125423 (2016).
- [74] I. V. Oladyskhin, S. B. Bodrov, Yu. A. Sergeev, A. I. Korytin, M. D. Tokman, and A. N. Stepanov, Optical emission of graphene and electron-hole pair production induced by a strong terahertz field, Phys. Rev. B. **96**, 155401 (2017).
- [75] Ch. Lui, K. F. Mak, J. Shan, and T. F. Heinz, Ultrafast Photoluminescence from Graphene, Phys. Rev. Lett. **105**, 127404 (2010).
- [76] S. Tani, F. Blanchard, and K. Tanaka, Ultrafast Carrier Dynamics in Graphene Under a High Electric Field, Phys. Rev. Lett. **109**, 166603 (2012).
- [77] T. Higuchi, C. Heide, K. Ullmann, H. B. Weber and P. Hommelhoff, Light-field-driven currents in graphene, Nature **550**, 224 (2017).
- [78] C. Heide, T. Higuchi, H. B. Weber and P. Hommelhoff, Coherent Electron Trajectory Control in Graphene, Phys. Rev. Lett. **121**, 207401 (2018).
- [79] S. M. Schmidt, D. Blaschke, G. Röpke, S. A. Smolyansky, A. V. Prozorkevich, A quantum kinetic equation for particle production in the Schwinger mechanism, Int. J. Mod. Phys. **E07**, 709 (1998).
- [80] Y. Kluger, E. Mottola, and J. M. Eisenberg, Quantum Vlasov equation and its Markov limit, Phys. Rev. D **58**, 125015 (1998).
- [81] S. M. Schmidt, D. Blaschke, G. Röpke, A. V. Prozorkevich, S. A. Smolyansky, V. D. Toneev, Non-Markovian effects in strong-field pair creation, Phys. Rev. D **59**, 094005 (1999).

- [82] S. A. Smolyansky, A. D. Panferov, D. Blaschke, and N. T. Gevorgyan, Kinetic equation approach to graphene in strong external fields, *Particles* **3**, 456 (2020).
- [83] S. P. Grivilov, D. M. Gitman, V. V. Dmitriev, A. D. Panferov, and S. A. Smolyansky, Radiation problems accompanying carrier production by an electric field in graphene, *Universe* **6**, 205 (2020).
- [84] A. Pierret, D. Mele, H. Graef, J. Palomo, T. Taniguchi, K. Watanabe, Y. Li, B. Toury, C. Journet, P. Steyer, V. Garnier, A. Loiseau, J. M. Berroir, E. Bocquillon, G. Fève, C. Voisin, E. Baudin, M. Rosticher, and B. Plaças, Dielectric permittivity, conductivity and breakdown field of hexagonal boron nitride, arXiv:2201.05826v2.
- [85] M. Abramowitz, and I. Stegun, *Handbook of mathematical functions* Dover Publications, New York, (1965).
- [86] S. P. Kim, and D. N. Page, Improved approximation for fermion pair production in inhomogeneous electric field, *Phys. Rev. D* **75**, 045013 (2007).
- [87] I. Akal, and G. G. Moortgat-Pick, Euclidean mirrors: enhanced vacuum decay from reflected instantons, *J. Phys. G* **45**, 055007 (2018).
- [88] F. W. J. Olver, D. W. Lozier, R. F. Boisvert, and C. W. Clark, *NIST Handbook of Mathematical Functions*, Cambridge University Press, England, (2010).
- [89] S. P. Grivilov, D. M. Gitman, and N. Yokomizo, Dirac fermions in strong electric field and quantum transport in graphene, *Phys. Rev. D* **86**, 125022 (2012).
- [90] Y. Kluger, J. M. Eisenberg, B. Svetitsky, F. Cooper, and E. Mottola, Pair production in a Strong Electric Field, *Phys. Rev. Lett.* **67**, 2427 (1991).
- [91] J. C. R. Bloch, V. A. Mizerny, A. V. Prozorkevich, C. D. Roberts, S. M. Schmidt, S. A. Smolyansky, and D. V. Vinnik, Pair creation: back reactions and dampings, *Phys. Rev. D* **60**, 116011 (1999).
- [92] A. Otto, D. Graevinger, and B. Kämpfer, Response of the QED(2) vacuum to a quench: Long-term oscillations of the electric field and the pair creation rate, *Plasma Phys. Control. Fusion* **61**, 074002 (2019).
- [93] See: <https://ekspla.com/product/nt200-nanosecond-tunable-dpss-lasers/>